Energy & Buildings 208 (2020) 109623

Contents lists available at ScienceDirect

Energy & Buildings

journal homepage: www.elsevier.com/locate/enbuild

Coloured building integrated photovoltaics: Influence on energy efficiency

Arne Røyset[a], Tore Kolås[a,*], Bjørn Petter Jelle[b,c]

[a] SINTEF Industry, NO-7465 Trondheim, Norway
[b] SINTEF Community, NO-7465 Trondheim, Norway
[c] Norwegian University of Science and Technology (NTNU), NO-7491 Trondheim, Norway

ARTICLE INFO

Article history:
Received 16 July 2019
Revised 1 November 2019
Accepted 19 November 2019
Available online 20 November 2019

Keywords:
Colour
Energy efficiency
Solar cell
Building integrated photovoltaics
BIPV

ABSTRACT

Building integrated photovoltaics (BIPV) has attracted increased commercial interest in recent years due to a growing focus on efficient utilization of land area and local renewable energy generation. Aesthetic aspects must be considered when photovoltaic panels are applied as building elements. Colours can be added by reflecting some of the sunlight that otherwise could have been utilized for electricity generation.

Reflectance spectra of commercial solar cell modules have been measured and analysed. Relative efficiency loss caused by the reflected solar radiation energy has been calculated. The calculated losses in efficiency based on measured spectra have been compared to model spectra with colour coordinates corresponding to RAL colours as well as more idealized monochromatic spectra.

The analysis shows that the most important colour parameter affecting loss is the lightness. The second most important parameter is the hue of the colour, with green-yellow colours having the lowest loss, and pink colours resulting in the highest loss, when colours with the same lightness are compared.

A Colour Performance Index (CPI) given by luminous reflectance divided by relative loss has been proposed as a figure of merit, thus allowing for a useful comparison of colours with different lightness.

1. Introduction

Building integrated photovoltaics (BIPV) can provide electricity to buildings and function both as an energy generator and a weather protection skin [1–6]. Acceptance by architects and other stakeholders in the building industry requires that the BIPV elements satisfy a wide range of aesthetic requirements such as size, shape, texture and colour [7–9]. Adding colour to an opaque black BIPV element requires that light is reflected from the module. Increased reflectance will reduce the photon flux available for current generation and thus an aesthetically pleasing surface may come at a cost of reduced electricity generation. A good understanding of the trade-off between choice of colour and energy efficiency will therefore be beneficial in order to satisfy both aesthetical and economical requirements. Such an understanding would enable architects, building contractors and house owners to make their decisions with respect to colours and power output of the BIPV systems based on quantified evaluations and data sets.

Several technologies have been introduced for adding colour to solar cell modules [10]. One of the most frequently reported techniques is the use of single and multilayer films that introduce spectrally selective reflectance due to interference [11–18]. A standard silicon (Si) solar cell has a single layer antireflection coating between the high index silicon and the low index encapsulation. This layer is designed to have a minimum reflection in the red part of the solar spectrum because this maximises the power conversion efficiency. Such a single layer typically leads to a dark blue appearance. Altering the refractive index or thickness of this layer can change the colour. Introducing multilayer coatings expands the range of possible colours that can be obtained. Other techniques for colouring include pigments printed on the cover glass [19–21], scattering and absorption added by plasmonic structures [22,23], quantum dots [24], photonic structures [25–27], and nanoscatterers [28].

Several authors have reported cell power conversion efficiency (PCE) measurements for various colours. Efficiencies ranged from 10.7 to 14.2% for 7 different colours created with a double layer

* Corresponding author.
E-mail address: tore.kolas@sintef.no (T. Kolås).

https://doi.org/10.1016/j.enbuild.2019.109623

antireflection coating (DLAR) [11]. Compared to 14.6% for a dark colour this corresponds to a relative power loss of 10 to 27%. DLAR was also used to create four colours, with PCE ranging from 16.1 to 17.0% [15]. Another DLAR experiment resulted in PCE values from 15.9 to 16.4% [16], but no reference was measured. The use of single and multilayer coating to produce 10 colours resulted in relative losses from 8 to 33% [12]. Four colours created by multilayer interference coatings [14] resulted in relative efficiency loss of 16 to 24%. A bright white colour created with a multilayer coating caused a relative loss of 40% [17]. Plasmonic colouring [23] obtained 9.6 to 12.2% relative loss and four printed colours [21] resulted in 20–25% relative loss. From the above results, it is very difficult if not impossible to properly compare different colours and obtain a conclusion on what is the preferred colour in order to minimize the reduction in power conversion efficiency. The main reason for this difficulty is that the lightness of the colours that was obtained are unknown. Increasing the lightness requires an increase in the reflectance, and this automatically causes the relative loss to increase. If we compare different colours with the same lightness, we may be able to conclude on which colour coordinates are favourable for reducing loss, for example hue and chroma of the colour. In addition to a lack of experimental comparison, a theoretical investigation of the impact of different colours on loss has also been missing.

Only recently, two studies have appeared that investigate the theoretical minimum efficiency loss in coloured solar cells, where the efficiency of the coloured cells are compared to the efficiency of a black reference cell [29,30]. Halme and Mäkinen [29] have analysed the efficiency by numerically simulating colours created by two flat-top spectral reflectance bands with band centre wavelengths and spectral widths as parameters. They found that when colours of equal relative luminosity were compared, the yellow-green colours were the most efficient colours. They explained this by the photopic sensitivity of the human eye. Peharz and Ulm [30] also analysed the efficiency loss by constructing flat-top spectral reflectance bands and analysed monochromatic colours and RAL colours. When analysing monochromatic 40 nm wide flat-top spectra they found that green colours were less efficient than blue and red colours. They also constructed pairs of flat-top spectral bands to match the RAL colour coordinates found from measurements of a catalogue of RAL colours [34]. In the monochromatic colour simulations, they found that blue colours were the most efficient ones. In an analysis of the measured RAL spectra, they found that blue, green, dark grey, brown and black had lower power loss than yellow, orange, red, violet, bright grey and white colours. The discrepancy between this result of Peharz and Ulm [30] and the result of Halme and Mäkinen [29] seems to stem from the fact that Peharz and Ulm did not compare colours with the same lightness or luminosity. The results from Peharz and Ulm with blue as the most efficient monochromatic colour arises because they have defined a colour efficiency as the ratio of the sum of X, Y and Z colour coordinates divided by current loss. By using $X+Y+Z$ rather than Y alone, Peharz and Ulm arrived at different conclusions as compared to Halme and Mäkinen. As we discuss later, we believe it is not appropriate to use $X+Y+Z$ when defining colour efficiency.

In our analysis we use the CIE XYZ, L*a*b and L*C*h° colour spaces to describe the colours. We follow the methodology of Halme and Mäkinen [29] and use Y to describe luminosity. We define a novel Colour Performance Index (CPI) as the ratio between reflected luminosity and relative power loss. We analyse measured spectra obtained from commercially available coloured solar cell modules. In addition, we investigate monochromatic colours created by flat-top reflectance spectra as well as more realistic model spectra that match RAL colour coordinates without having steep spectral features. Thus, we arrive at results for both flat-top and more realistic spectra. We apply the L*a*b* and L*C*h° colour spaces due to their perceptual uniformity. Lightness L*, chroma C, and hue h°, closely matches the human perception of colours. We demonstrate that lightness is the most important parameter to keep losses low. Hue is the second most important parameter, and the results demonstrate that green colours are more efficient than blue and red colours. In our analysis we also put special attention to the loss contribution from the near infrared (NIR) reflectance part of the solar spectrum. From this combined investigation of measured and modelled spectra we arrive at results that can be used as guidelines in the prediction of how the efficiency of BIPV solar modules is affected by the choice of colour.

2. Materials and methods

From different suppliers we received a total of 15 samples of commercially available coloured solar cell modules, see Table 1 and Fig. 1. All modules are based on crystalline silicon, while different technologies are used for the colour generation. All efficiencies reported in the table are given by the suppliers. The received modules were not electrically connected, and independent power measurements could therefore not be carried out.

Samples 1–8 were supplied by the company LOF Solar (Taiwan). The colour is here obtained by adding an extra colour modulating layer on top of the original antireflection layer on the silicon solar cells. According to Shih et al. [10], the material of the extra layer can be for example SiO_2, MgF_2 or Si_3N_4.

Sample 9 and 10 both use technology developed by Solaxess (Switzerland). Here two different elements are combined: (1) a solar cell technology able to convert solar infrared light into electricity (crystalline silicon solar cells) and (2) a selective filter which reflects and diffuse the visible spectrum while transmitting infrared. The modules present a white aspect, demonstrating that PV elements can become virtually hidden energy sources in buildings [17].

Sample 11 is an example of the so-called Kromatix technology developed by the company Swissinso (Switzerland). Here, a multilayered coating is deposited on the inner surface of the cover glass. According to the company website, no pigments or dyes (paint) are used so that the colour does not fade out with the passage of time

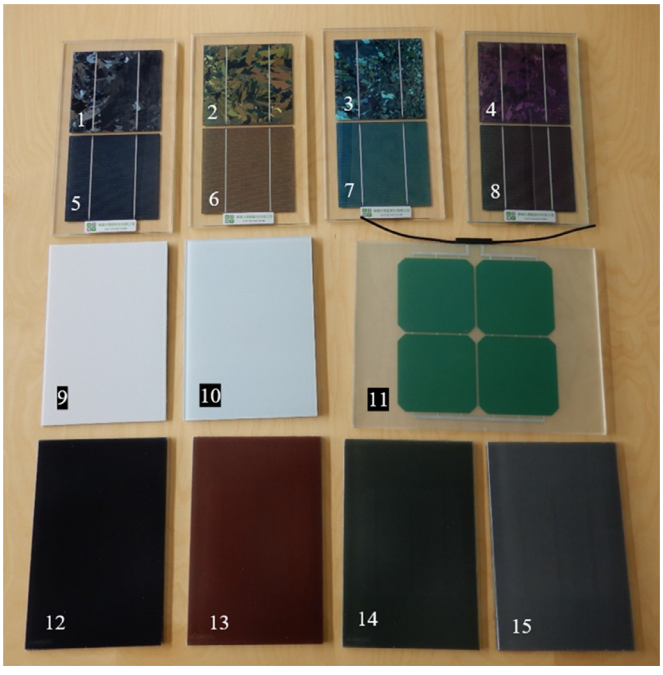

Fig. 1. Photograph of measured solar cell modules with different colours.

Table 1
Measured commercial crystalline silicon solar cell modules with different colours. .

Sample number	Name/colour	Sample supplier	Efficiency [%]*	Literature reference
1	Stone Elegance	LOF Solar	15.0–17.8	[10]
2	Metallic Gold	LOF Solar	15.2–17.0	[10]
3	Emerald Green	LOF Solar	15.2–17.6	[10]
4	Disco Pink	LOF Solar	15.0–17.6	[10]
5	True Steel	LOF Solar	16.4–17.4	[10]
6	Tile Red	LOF Solar	16.4–17.2	[10]
7	Forest Green	LOF Solar	16.4–17.4	[10]
8	Lavender	LOF Solar	16.4–17.2	[10]
9	Vivid White	Solaxess	10.6	[17]
10	White	Issol	9.0	
11	Kromatix Green	ML System	–	[8,14]
12	Anthracite	Sunage	14.5	
13	Terracotta	Sunage	16.7	
14	Green Moss	Sunage	16.7	
15	Light Grey	Sunage	16.7	

* Module efficiency values provided by sample supplier.

or due to sun exposure. Some investigations of this BIPV technology has been reported in the literature [8,14].

Samples 12–15 demonstrate the technology developed by the company Sunage (Switzerland). According to the company they use a new process for mineral coating, which is fixed onto the surface of the cover glass at a very high temperature, thus becoming structurally part of the glass. It is not clear how much absorption loss is introduced by this process in the visible or in the near infrared. If we look at the efficiencies given by the supplier in Table 1, we see that the darkest module with the colour Anthracite (sample 12) actually gives the lowest efficiency. This method of producing coloured modules may therefore be best suited for lighter colours.

Spectral reflectance of the coloured solar modules was measured with a PerkinElmer 1050 spectrophotometer using an 8° incident angle and a 150 mm integrating sphere accessory, where the total (specular + diffuse) reflectance was recorded. The spectra were recorded from 280 to 2500 nm in 5 nm increments. Only the spectral range between 300–1200 nm was used in the calculations. Some of the modules have spatially varying reflectance, and the reflectance was therefore calculated as the average reflectance from 2–5 measurement positions on the module.

For colour calculations the CIE XYZ, L*a*b* and L*C*h° colour spaces [31,32] have been used. The XYZ tristimulus values are given by

$$X = \frac{K}{N}\int_{380}^{780} R(\lambda)\ S(\lambda)\ \bar{x}(\lambda)\ d\lambda \tag{1}$$

$$Y = \frac{K}{N}\int_{380}^{780} R(\lambda)\ S(\lambda)\ \bar{y}(\lambda)\ d\lambda \tag{2}$$

$$Z = \frac{K}{N}\int_{380}^{780} R(\lambda)\ S(\lambda)\bar{z}(\lambda)\ d\lambda \tag{3}$$

$$N = \int_{380}^{780} S(\lambda)\ \bar{y}(\lambda)\ d\lambda \tag{4}$$

where $\bar{x}(\lambda)$, $\bar{y}(\lambda)$ and $\bar{z}(\lambda)$ are the colour matching functions, R(λ) is the reflectance, S(λ) is the illuminant spectrum, and K is a normalization factor, usually 1 or 100. We have used $K = 1$ as normalization factor, CIE 1931 2° observer for the colour matching functions, and D65 as illuminant (Fig. 2). The D65 is defined by CIE and is intended to represent daylight illumination. The colour matching function $\bar{y}(\lambda)$ equals the photopic luminosity function (eye sensitivity), and Y therefore also represents the luminous reflectance factor.

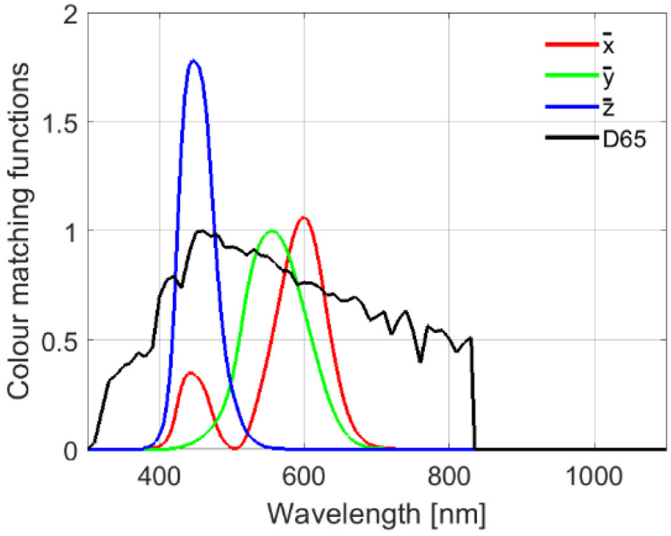

Fig. 2. Colour matching functions and D65 illuminant used in the calculations.

For display in a chromaticity diagram, the x(λ), y(λ) and z(λ) chromaticity values are useful. They are given by

$$x = \frac{X}{X+Y+Z} \tag{5}$$

$$y = \frac{Y}{X+Y+Z} \tag{6}$$

$$z = \frac{Z}{X+Y+Z} \tag{7}$$

We also use the CIE 1976 L*a*b* colour space which is a three dimensional, approximately uniform colour space produced by plotting L*, a*, b* in a rectangular coordinate system. The coordinates L*, a*, b* are given by

$$L^* = 116\ f\left(\frac{Y}{Y_N}\right) - 16 \tag{8}$$

$$a^* = 500\left(f\left(\frac{Y}{Y_N}\right) - f\left(\frac{X}{X_N}\right)\right) \tag{9}$$

$$b^* = 200\left(f\left(\frac{Y}{Y_N}\right) - f\left(\frac{Z}{Z_N}\right)\right) \tag{10}$$

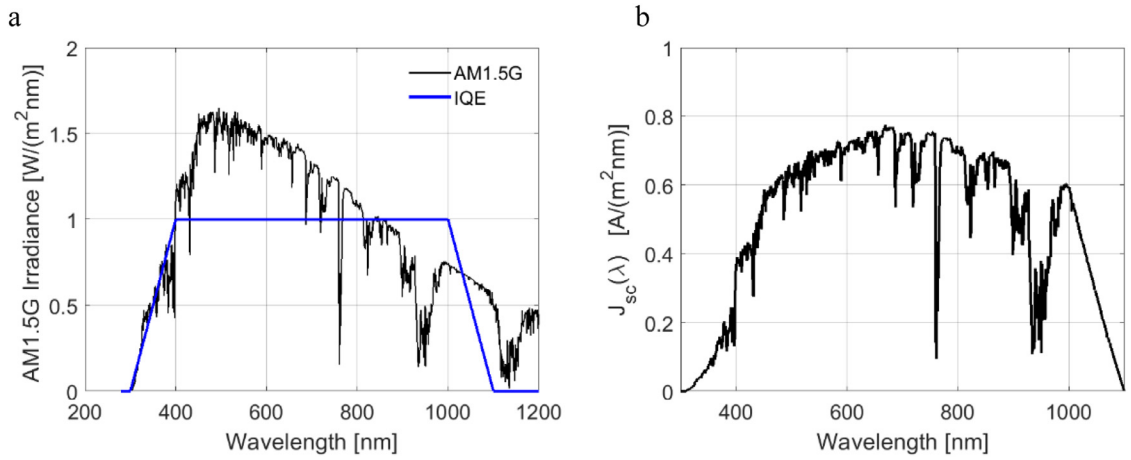

Fig. 3. (a) Solar irradiance spectrum and internal quantum efficiency used in the calculations. (b) The resulting photocurrent density $J_{sc}(\lambda)$ spectral dependence.

where

$$f(t) = \begin{cases} t^{1/3} & if\ t > \left(\frac{6}{29}\right)^3 \\ \frac{1}{3}\left(\frac{29}{6}\right)^2 t + \frac{4}{29} & if\ t < \left(\frac{6}{29}\right)^3 \end{cases} \quad (11)$$

The cube root relation holds for $L>8$, $Y>0.0089$ which is the case for all practical PV modules. The normalization factors in the case of D65 illumination are $X_N = 0.95047$, $Y_N = 1.00$, and $Z_N = 1.08883$. $a^* = 0$ and $b^* = 0$ represent grey while green to red are represented along the a^* axis and blue to yellow are represented along the b^* axis. The $L^*a^*b^*$ colour space can also be expressed in terms of chroma C, saturation S^*, and hue h° (CIE $L^*C^*h^\circ$) where the hue angle ranges from 0° (red/magenta) via 90° (yellow), 180° (green) and 270° (blue).

$$C^* = \sqrt{a^{*2} + b^{*2}} \quad (12)$$

$$S^* = \frac{C^*}{L^*} \quad (13)$$

$$h^\circ = arctan\left(\frac{b^*}{a^*}\right) \quad (14)$$

The CIE $L^*a^*b^*$ colour space is designed to be perceptually uniform, unlike the RGB and CMYK colour space. The L^*, C^*, h° closely matches human perception of lightness, chroma and hue. Equal step changes in lightness L^* represents equal step changes in perceived lightness and may therefore be most useful for displaying the impact of lightness on efficiency loss.

The energy generation is modelled by calculating the short circuit photocurrent density J_{sc} as [33]:

$$J_{sc} = \int_{300}^{1200} \frac{q\lambda}{hc}(1 - A(\lambda) - R(\lambda))\ I(\lambda)\ IQE(\lambda)\ d\lambda \quad (15)$$

where $I(\lambda)$ is the AM1.5 G standard solar irradiance spectrum, $IQE(\lambda)$ is the internal quantum efficiency, q is the electron charge, λ/hc is the photon energy, $R(\lambda)$ is the total hemispherical spectral reflectance, and $A(\lambda)$ is the parasitic loss in front cover, encapsulation, antireflection coating and any possible colouring layers. This model neglects the influence of finite charge carrier diffusion lengths and series resistance. We also omit the influence of circuit voltage on the efficiency. It was found that the variation in J_{sc} was a good approximation for the variation in efficiency for coloured solar cells [29]. The model we have used for the IQE displayed in Fig. 3a is intended to represent a crystalline silicon solar cell. The IQE is set to 100% (one electron per photon) in the 400–1000 nm spectral band and decreasing in the UV region and near the 1100 nm bandgap. The spectral dependence of $J_{sc}(\lambda)$ in the case $R=0$, $A=0$ is given in Fig. 3b.

We introduce a relative efficiency E and relative loss P given by

$$E = 1 - P = \frac{J_{sc}}{J_{sc,ref}} \quad (16)$$

where $J_{sc,ref}$ is the photocurrent density in the case $A(\lambda)=0$ and $R(\lambda)=0$. In the following we assume the lossless case $A(\lambda)=0$ and we can write the relative loss as:

$$P = \frac{\int_{300}^{1200} \lambda\ R(\lambda)\ I(\lambda) IQE(\lambda)\ d\lambda}{\int_{300}^{1200} \lambda\ I(\lambda)\ IQE(\lambda)\ d\lambda} \quad (17)$$

For the discussion of different contributions to loss we divide the total relative loss P into P_{UV}, P_{VIS}, and P_{NIR}, which are the loss contributions from the ultraviolet (UV) (300–400 nm), visible (VIS) (400–700 nm) and near infrared (NIR) (700–1200 nm) wavelength regions, respectively:

$$P = P_{UV} + P_{VIS} + P_{NIR} \quad (18)$$

Although the eye sensitivity $\bar{y}(\lambda)$ applied in Eq. (2) is nonzero in the range from 380 to 780 nm (Eq. (2)), the sensitivity outside 400–700 nm is so low that it is useful to apply a VIS range of 400–700 nm for this relative loss analysis. The contributions to loss in the UV and NIR regions are due to unwanted reflectance in these spectral bands. With our model (Eq. (15)) the relative contribution to $J_{sc,ref}$ from the UV, VIS, and NIR regions are $F_{UV} = 2.2\%$, $F_{VIS} = 47.2\%$, and $F_{NIR} = 50.6\%$, respectively. These numbers are only valid for the present model with an IQE intended to be representative for crystalline silicon cells. Other materials with different bandgaps and spectral shape of IQE will have a different spectral sensitivity to the photocurrent density (Fig. 3b), and hence the relative loss caused by a spectral reflectance will be different. However, the methodology we apply may still be applicable by using another spectral dependence of IQE.

A reflectance larger than zero is needed in the visible spectral band in order to create a colour. A higher reflectance increases both the luminous reflectance Y and the relative loss P. We therefore propose a colour performance index (CPI), the relation Y/P, as a useful figure of merit for comparison of efficiency loss in coloured photovoltaics:

$$CPI = \frac{Y}{P} \quad (19)$$

This definition of CPI allows for comparison of colours with different lightness. If we consider a case with the same spectral reflectance across all wavelengths (grey), we get CPI = 1, independent of the magnitude of R. By increasing the reflectance in the VIS and reducing the reflectance in NIR, we can increase the CPI to be larger than 1. CPI can be maximized by having reflectance where the eye sensitivity $\bar{y}(\lambda)$ is largest, and zero reflectance outside this band. A second CPI may also be useful, for comparison of the VIS part of the spectrum only: $CPI_{VIS} = Y/P_{VIS}$, where only the loss in the visible range (400–700 nm) is considered.

In addition to the evaluation of the measured spectra from the 15 commercial modules, we also calculated colour coordinates and loss based on 40 and 80 nm wide flat-top reflectance spectra with varying centre wavelength. These spectra represent highly saturated (high chroma) colours. For comparison to more common colours, we have also used tabulated L*a*b* values of a large number of RAL colours [34] and numerically computed reflectance spectra that matches these colour coordinates. The computation procedure is to model a reflectance spectrum with five spectral reflectance's (R_0, R_1, R_2, R_3, R_4) at wavelengths 400, 450, 550, 600 and 700 nm. The reflectance values at wavelengths up to $\lambda_0 = 400$ nm and at wavelength $\lambda_4 = 700$ nm and above are fixed at a low value (4%) while R1, R2 and R3 are determined by the colour coordinate requirement. The spectral transition from R_n to R_{n+1} is given by

$$R(\lambda) = R_n + (R_{n+1} - R_n)\ sin^2\left(\frac{\pi}{2}\frac{\lambda - \lambda_n}{\lambda_{n+1} - \lambda_n}\right) \tag{20}$$

in order to have reflectance spectra with slowly varying spectral features. Chromaticity values X, Y, Z are computed from L*, a*, b* and the required R_1, R_2 and R_3 are calculated based on a transfer matrix $[R_1, R_2, R_3]^T = M^*[X, Y, Z]^T$. This selection of spectral model is motivated by ease of calculation and the advantage of having a linear relationship between X, Y, Z and the spectral reflectance parameters. A further advantage is that we also have a linear relationship from X, Y, Z to the relative loss within these spectral bands given by

$$P = \begin{bmatrix} dP/dX \\ dP/dY \\ dP/dZ \end{bmatrix} \begin{bmatrix} X \\ Y \\ Z \end{bmatrix} \tag{21}$$

Another advantage is that the spectral transitions are more realistic than having flat top spectral bands. A disadvantage with this approach is that not all colour coordinates can be achieved. The transition wavelengths $\lambda_1 = 450$ nm $\lambda_2 = 550$ nm $\lambda_3 = 600$ nm were optimum for maximizing the number of realized RAL spectra. The number of spectra that was obtained were also limited by not allowing reflectance higher than 80% and not lower than 4%. With the given model 160 out of the 212 RAL colours were realized. The transfer matrix M = [0.15, −0.25, 1.13; −1.53, 2.42, −0.03; 2.77, −1.09, −0.36] was obtained and dP/dX = 0.198, dP/dY = 0.125, and dP/dZ = 0.066.

3. Results

The results from spectral reflectance measurements on 15 different commercial coloured solar modules are given in Fig. 4, with the total (specular + diffuse) reflectance depicted. Colour coordinates and relative losses P were calculated and are displayed in Table 2 together with the CPI and CPI_{VIS}

The relation between calculated relative loss P and lightness L* is displayed in Fig. 5. The lightness ranges from L* = 29.6 (Y = 0.061) to L* = 70.6 (Y = 0.671) while the estimated relative loss P varies from 6.4% to 45.2%.

Several observations can be made from the acquired spectra. Firstly, the reflectance is always larger than 5% in the entire spectrum. This may be caused by Fresnel reflection of the cover glass. This baseline reflectance causes an increased loss in the NIR band while in the VIS band it also reduces the chroma of the colour, as it tends to move all colours towards grey. As can be seen from Table 2, the chroma values are less than 15 for most of the solar modules. For green colours, an increased baseline reflectance in the blue and red part of the spectrum will reduce chroma and slightly increase lightness, but most importantly reduce module efficiency. Secondly, we observe that most of the modules have a NIR reflectance that is much higher than 5%. The variation in P_{NIR} contributes strongly to the variation in relative efficiency loss P. This is clear from Fig. 6 where we compare P_{NIR} and P_{VIS}. The magnitude of variation in P_{NIR} is comparable to the variation in P_{VIS}.

It is illustrative to compare the calculated loss based on measured spectra to the calculated loss of three different model spectra.

A first model spectrum (grey in UV–VIS-NIR) is the case of constant reflectance in the entire spectral band ($R_{UV} = R_{VIS} = R_{NIR}$). The lightness is here varied by varying the reflectance.

A second model spectrum (grey in VIS) is when we only vary the grey reflectance in the VIS spectral region (400–700 nm) while keeping the UV and NIR reflectance constant at 4%. The motivation to keep a nonzero reflectance outside the main reflection band is to study the impact of unintentional interface or surface reflectance such as the air-glass interface.

A third model spectrum (minimum loss) is the case of a narrow flat-top spectral band centred at 545 nm with 100% reflectance within the band and 0% reflectance outside the band. The lightness is here varied by increasing the width of the band. This case represents the minimum loss that can be obtained for a given lightness. The colour of the Minimum loss case is green-yellow and varies slightly with the lightness.

Examples of the model spectra are displayed in Fig. 7. The reflectance amplitude (R = 0.18) of the grey spectra and the spectral width (19 nm) of the minimum loss spectrum are selected to result in a medium lightness L* = 50.

In Fig. 8 the results from the three spectral models are compared with the results from the 15 measured spectra.

It is observed that the calculated loss based on the 15 measured spectra is always higher than the grey in VIS case. This corresponds to the observation that high NIR reflectance provides a strong contribution to the total loss. A few of the samples have a NIR reflectance that is higher than the VIS reflectance. For these samples the loss is higher than the grey in UV–VIS-NIR case. The results show as expected a strong correlation between lightness and relative loss.

The motivation for our proposed colour performance index (CPI = Y/P) is to better compare colours with different lightness. The CPI of the measured and modelled cases are shown in Fig. 9.

The grey in UV–VIS-NIR model case has a CPI of 1, independent of the lightness value.

The Grey in VIS case ($R_{UV} = R_{NIR}$ = 4%) increases the CPI up to 2.03, depending on the lightness value. For low lightness values the relative impact of the 4% UV-NIR baseline reflectance becomes substantial. If we had reduced both R_{UV} and R_{NIR} to 0%, the CPI would have increased further to 2.13 and also been independent of the lightness value.

The CPI for these two grey cases may be expressed by the reference photocurrent fractions F_{UV} = 2.2%, F_{VIS} = 47.2%, F_{NIR} = 50.6%, and reflectance values R_{UV}, R_{VIS}, R_{NIR} as:

$$CPI = \frac{Y}{P} = \frac{R_{VIS}}{F_{UV}\ R_{UV} + F_{VIS}\ R_{VIS} + F_{NIR}\ R_{NIR}} \tag{22}$$

In both of the grey cases the colour performance index for the visible part of the spectrum can be expressed as: $CPI_{VIS} = 1/F_{VIS} = 2.13$.

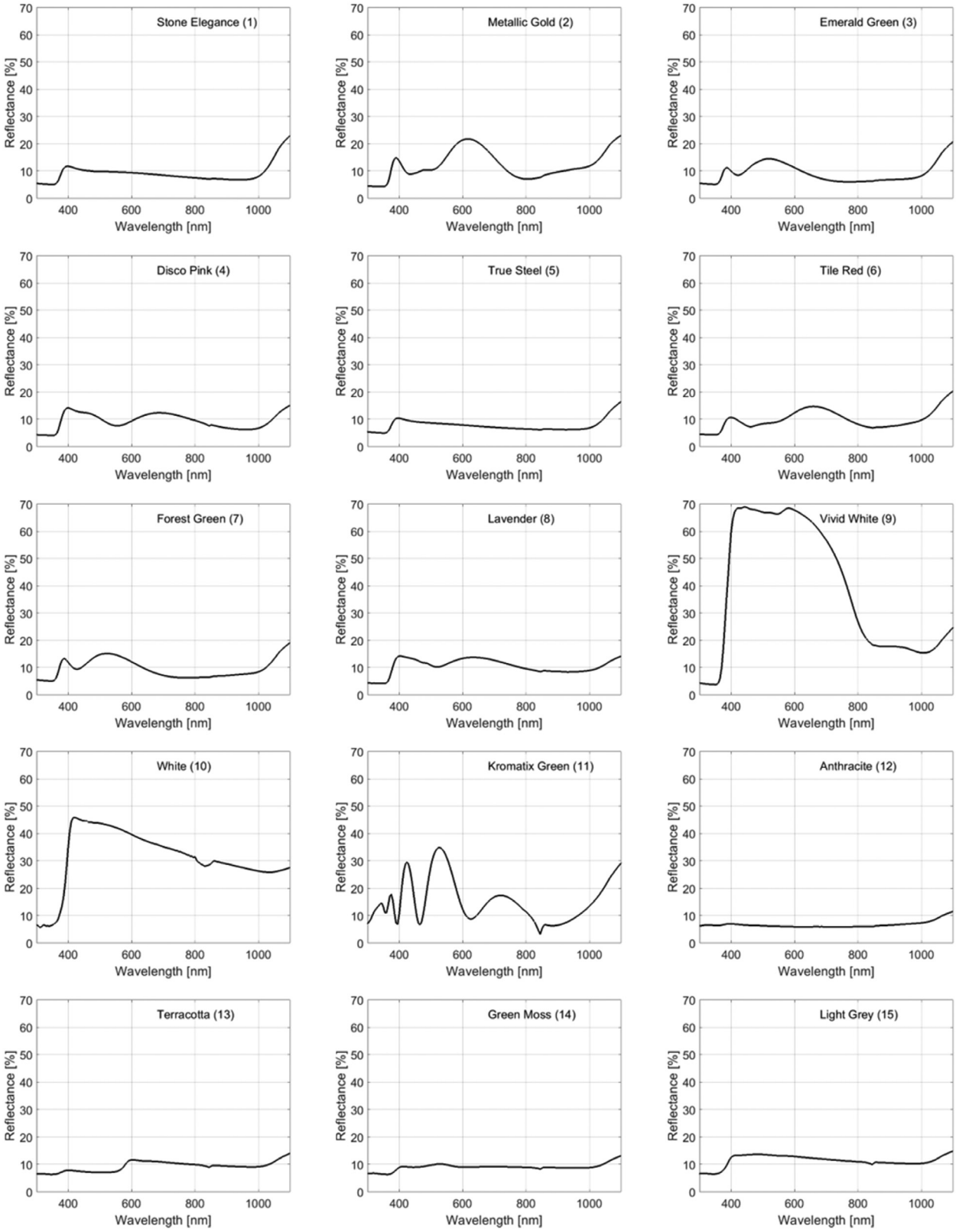

Fig. 4. Measured reflectance spectra for 15 commercially available coloured modules. The dip in some of the spectra near 860 nm is an artefact of the instrumentation (detector shift).

Table 2
Calculated colour coordinates, relative losses, and colour performance index based on measured reflectance spectra.

Sample		Colour										Relative loss [%]			CPI	
		X	Y	Z	x	y	L	a	b	Chroma	Hue	P	P_{VIS}	P_{NIR}	Y/P_{VIS}	Y/P
1	Stone Elegance	0.09	0.10	0.11	0.30	0.32	37.1	−0.2	−2.1	2.2	264	8.8	4.5	4.1	2.12	1.09
2	Metallic Gold	0.17	0.16	0.11	0.39	0.37	47.1	8.5	17.0	19.0	63	12.8	7.4	5.2	2.18	1.26
3	Emerald Green	0.11	0.13	0.12	0.30	0.36	42.6	−10.7	5.2	11.9	154	9.1	5.2	3.7	2.48	1.42
4	Disco Pink	0.09	0.09	0.13	0.30	0.28	35.7	8.2	−10.1	13.0	309	9.7	5.0	4.5	1.77	0.91
5	True Steel	0.08	0.08	0.10	0.30	0.32	34.5	−0.5	−3.0	3.1	260	7.5	3.9	3.5	2.12	1.09
6	Tile red	0.11	0.10	0.09	0.36	0.34	38.1	7.6	6.9	10.3	42	10.2	5.2	4.8	1.94	0.99
7	Forest Green	0.11	0.14	0.12	0.30	0.36	43.8	−10.5	5.9	12.1	151	9.5	5.5	3.8	2.48	1.44
8	Lavender	0.12	0.12	0.14	0.32	0.31	41.0	6.9	−2.2	7.2	342	11.1	5.9	4.9	2.00	1.07
9	Vivid White	0.64	0.67	0.74	0.31	0.33	85.5	0.2	−0.9	0.9	284	45.2	31.1	13.5	2.16	1.48
10	White	0.39	0.42	0.48	0.30	0.32	70.6	−2.4	−3.4	4.1	235	34.7	19.2	15.1	2.16	1.20
11	Kromatix Green	0.16	0.24	0.19	0.28	0.41	56.5	−34.2	14.0	36.9	158	15.2	8.9	6.0	2.73	1.60
12	Anthracite	0.06	0.06	0.07	0.30	0.32	29.6	0.0	−1.8	1.8	271	6.4	2.9	3.3	2.10	0.96
13	Terracotta	0.09	0.09	0.08	0.36	0.33	35.2	8.7	4.6	9.9	28	9.4	4.3	5.0	1.99	0.91
14	Green Moss	0.09	0.10	0.10	0.31	0.34	37.0	−2.9	1.4	3.3	154	9.1	4.4	4.6	2.17	1.05
15	Light Grey	0.12	0.13	0.15	0.31	0.33	43.0	−1.0	−0.8	1.3	220	11.8	6.1	5.5	2.15	1.11

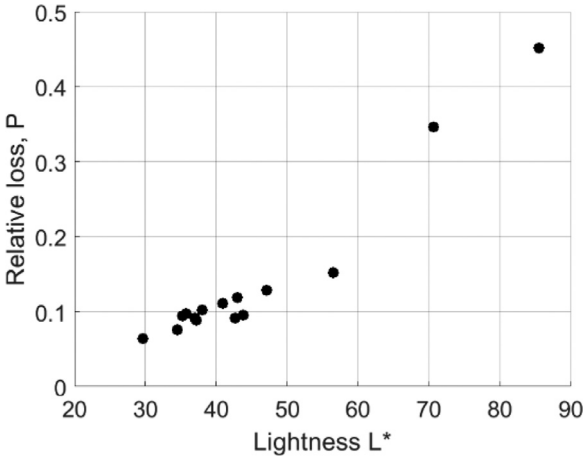

Fig. 5. Calculated relative loss (P) versus lightness (L^*) for the measured spectra.

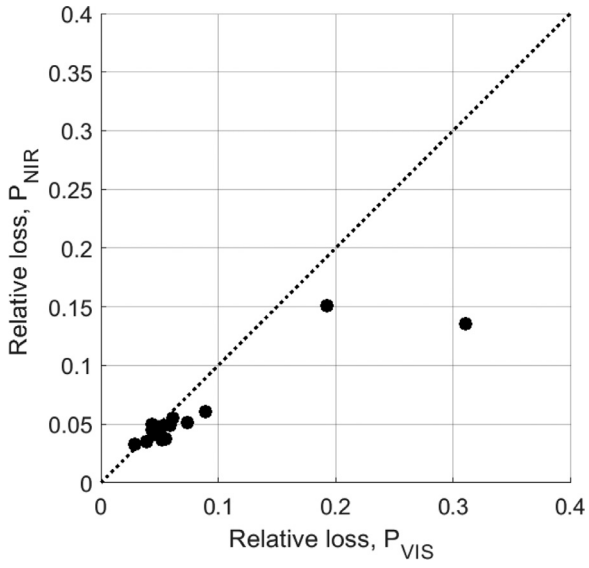

Fig. 6. Comparison of contribution from VIS and NIR reflectance to relative efficiency loss P_{VIS} and P_{NIR}. The dotted line indicates that the relative loss is equal in VIS and NIR.

The CPI of our measured spectra ranges from 0.91 to 1.6. This is comparable to the grey in UV–VIS-NIR case, but always lower than the grey in VIS case.

The CPI for the minimum loss case is in general much higher than any of the other cases. However, for very high lightness ($L^* = 100$) the CPI for the minimum loss case is reduced to 2.13. The maximum CPI is approximately 5.75 and is approached when the reflection band gets narrow (reduced lightness). This number may also be found by inspecting the spectral dependence of Y and J_{sc}, given by Eqs. (2) and (15). This relation is plotted in Fig. 10 and shows that the optimum wavelengths are close to the peak of the eye sensitivity $\bar{y}(\lambda)$ at 555 nm, but slightly blue-shifted due to the λ dependence on J_{sc} and a slight difference between D65 and AM1.5 G spectra.

Fig. 9 demonstrates that different colours may have substantial differences in the relative loss P. Blue, green and red colours are compared to grey in Fig. 11a. The colours are created by monochromatic 80 nm wide flat-top spectra centred at 480, 545 and 630 nm, respectively. The lightness is varied by increasing the band reflectance from 4 to 100%. The red and blue colours have a limited lightness due to limited spectral width and the fact that the wavelengths corresponding to red and blue colours have a relatively low eye sensitivity.

Outside the reflectance band, the baseline reflectance is constant at 4%. This is a more realistic spectrum than the minimum loss spectrum (Fig. 7) that has a baseline reflectance of 0%. In Fig. 11a, the relative loss in the visible spectral band (P_{VIS}) is dis-

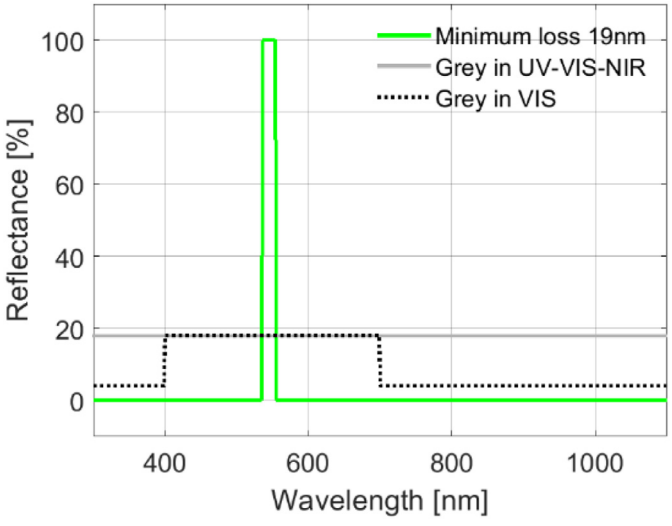

Fig. 7. Examples of model spectra, all having a lightness $L^* = 50$ (corresponding to $Y = 0.18$).

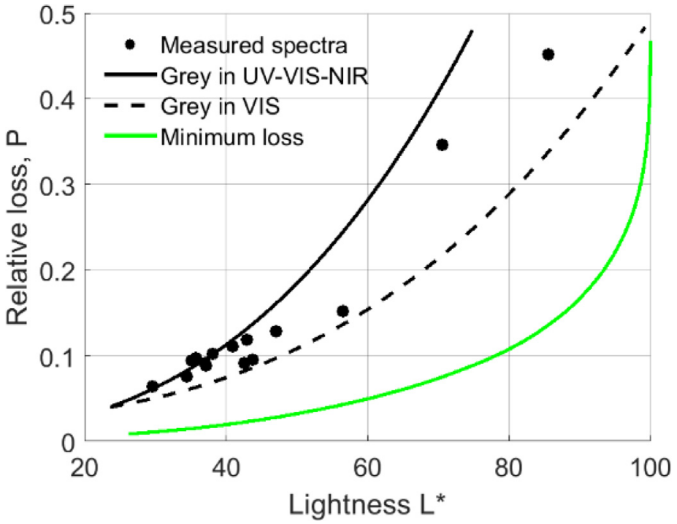

Fig. 8. Calculated relative loss versus lightness for 15 measured spectra compared with three model cases.

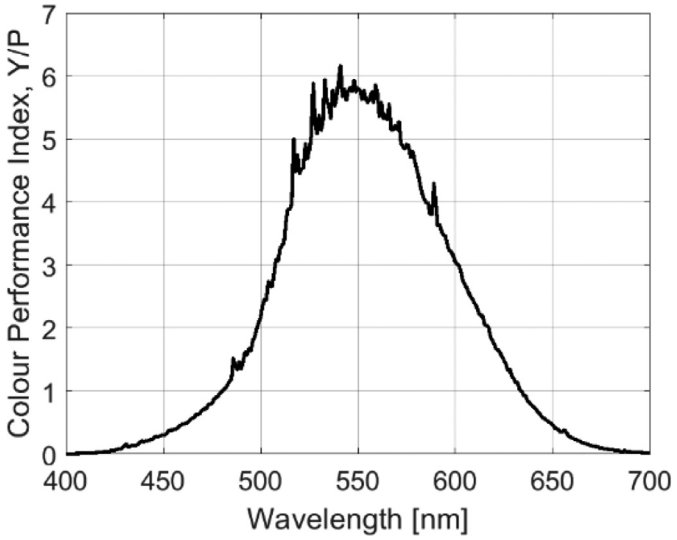

Fig. 10. Maximum CPI obtained in the limit of a narrow spectral band of 1 nm width.

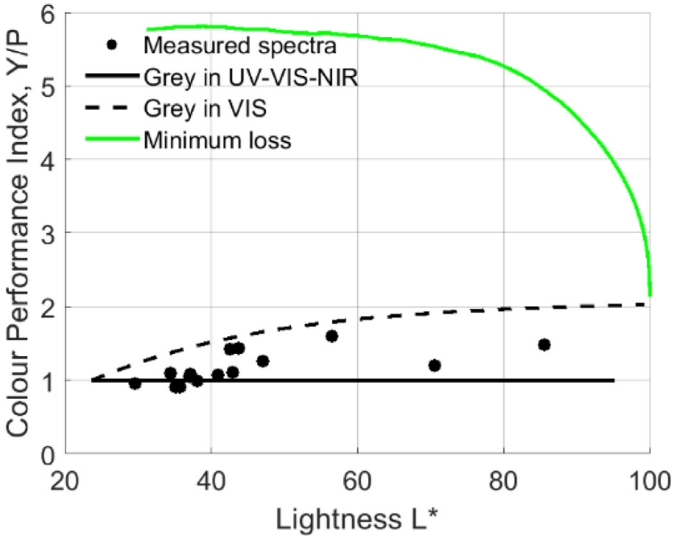

Fig. 9. Colour performance index Y/P calculated for the measured and modelled cases.

played. The corresponding CPI_{VIS} is displayed in Fig. 11b, and includes the loss in the visible part of the spectrum, which is the spectral region that is most affected by the choice of colour.

Examples of the model spectra are displayed in Fig. 12. The reflectance level corresponds to a lightness $L^* = 50$ for all of the five spectra. It can be seen that for the same lightness the reflectance level of green is much lower than blue and red. This is due to the high eye sensitivity in the green region. The reflectance level in grey is even lower. This is due to the wider spectral width.

A further analysis of even more realistic model spectra was carried out by constructing spectra with colour coordinates matching 160 classic RAL colours [34]. The calculation procedure of the RAL spectra is described in paragraph 2. Examples of spectra are displayed in Fig. 13 for RAL 5015 Sky blue, RAL 6024 Traffic green, RAL 4005 Blue lilac, and RAL 7005 Mouse grey. These colours all have a lightness close to $L = 50$.

The relative loss P_{VIS} is plotted in Fig. 14a together with the results obtained for 80 nm wide flat-top spectra and the CPI is given in Fig. 14b. The results show that most of the RAL spectra perform better than the grey case, which can be explained by a reduced reflectance near 400 and 700 nm, see Fig. 13.

The reason why RAL model spectra perform worse than the flat-top 80 nm green case is due to the less steep spectral edges,

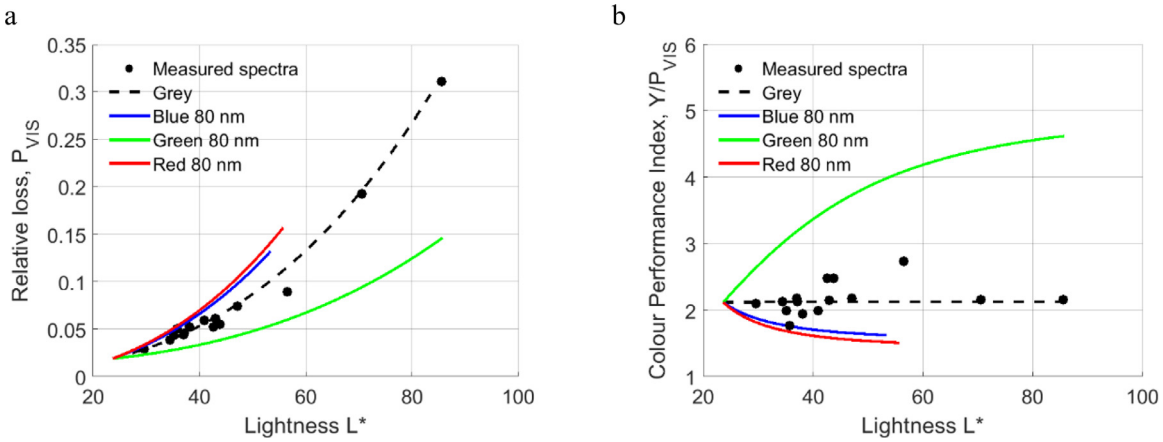

Fig. 11. Comparison of relative loss P_{VIS} (a) and CPI_{VIS} (b) for measured colours and model blue, green and red colours. The model colours are created with 80 nm wide flat-top spectral bands centred at 480, 545, and 630 nm respectively, with 4% baseline reflectance outside the band.

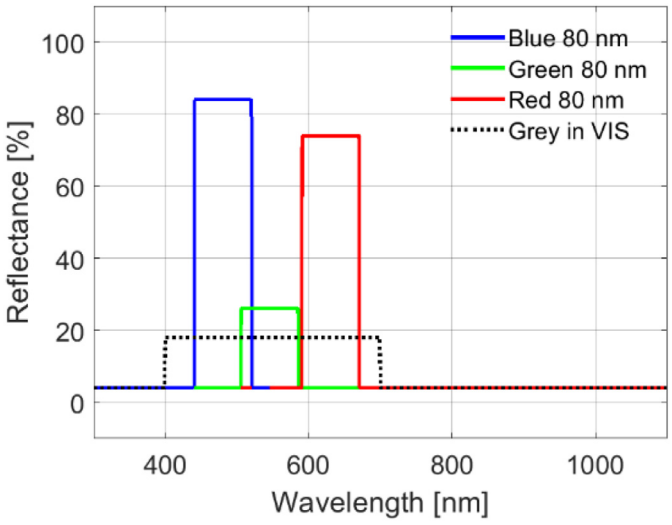

Fig. 12. Examples of model spectra used in the calculations. The reflectance level corresponds to a lightness $L^* = 50$ ($Y = 0.18$).

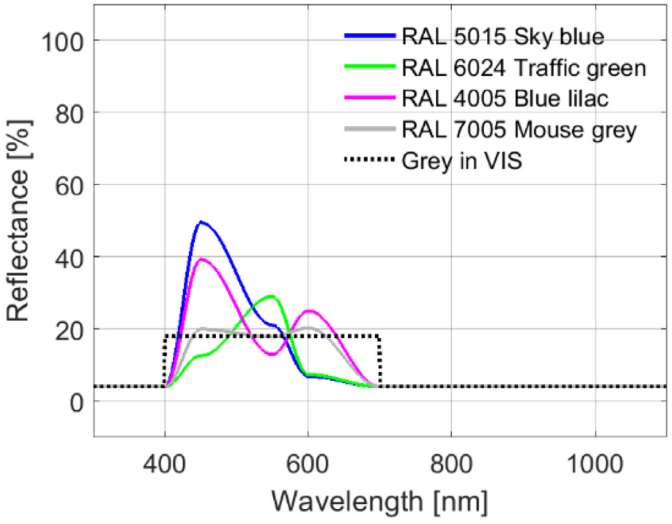

Fig. 13. Example of four model RAL spectra together with grey in VIS spectrum. All of these spectra provide lightness L^* close to 50.

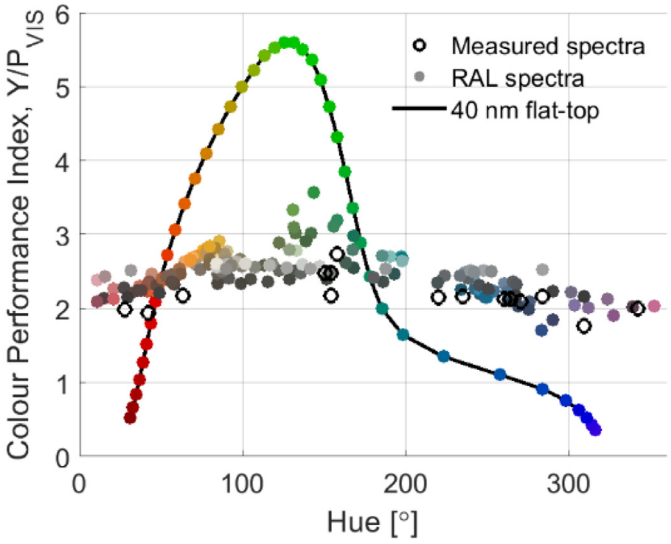

Fig. 15. Colour performance index versus hue for measured spectra, computed RAL spectra, and 40 nm flat-top spectra. The colours of the 40 nm flat-top spectra are shown with 5 nm increment in centre wavelength.

also indicating that higher chroma, or more saturated colours may give better results. On the other hand, the higher loss of the flat-top 80 nm red and blue colours, indicate the opposite. The reason for this is that the hue of the colour determines whether high chroma is an advantage or not. High chroma reduces loss for orange-yellow-green colours while for red-pink-blue colours, an increased chroma results in increased loss.

The impact of hue was investigated with spectra composed of a 40 nm flat-top spectral band with 100% reflectance inside band and 0% reflectance outside the band. The hue was varied by varying the centre wavelength of the reflectance band. These spectra result in colours that are highly saturated (high chroma).

In Fig. 15 the CPI_{VIS} has been plotted versus hue for the flat-top spectra together with results from the RAL spectra. For the 40 nm flat-top spectra the benefit of having a hue between approximately 60° and 160° can be clearly seen. From this we can conclude that high chroma improves CPI only for orange-yellow-green colours. The highest CPI for 40 nm flat-top are obtained with a centre wavelength between 545 and 550 nm, in good agreement with the prediction of Fig. 10.

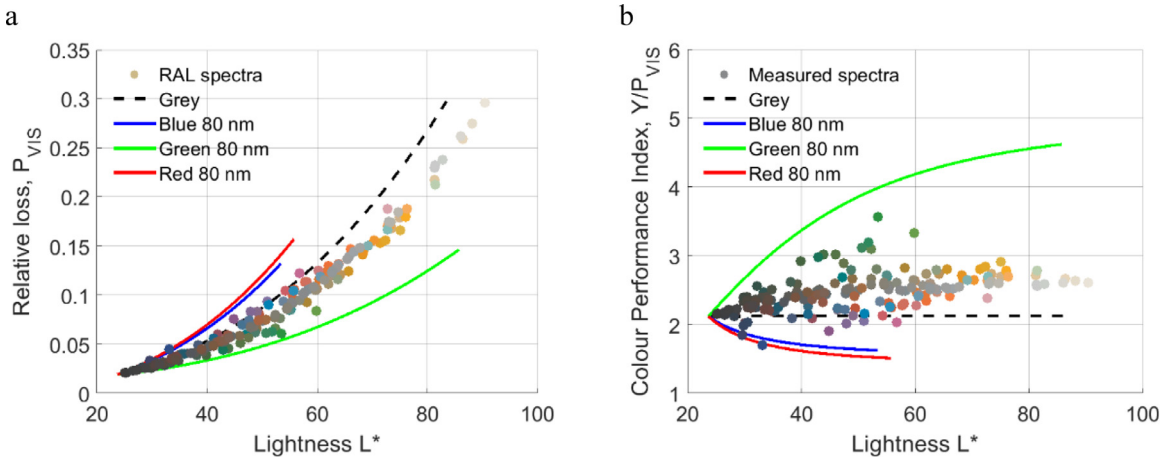

Fig. 14. Relative loss P_{VIS} and CPI_{VIS} computed from RAL spectra and model grey, blue, green and red colours. The model colours are created with 80 nm wide flat-top spectral bands centred at 480, 545, and 630 nm respectively, with 4% baseline reflectance outside the band. The colouring of the dots representing RAL results are based on the sRGB values of that RAL colour.

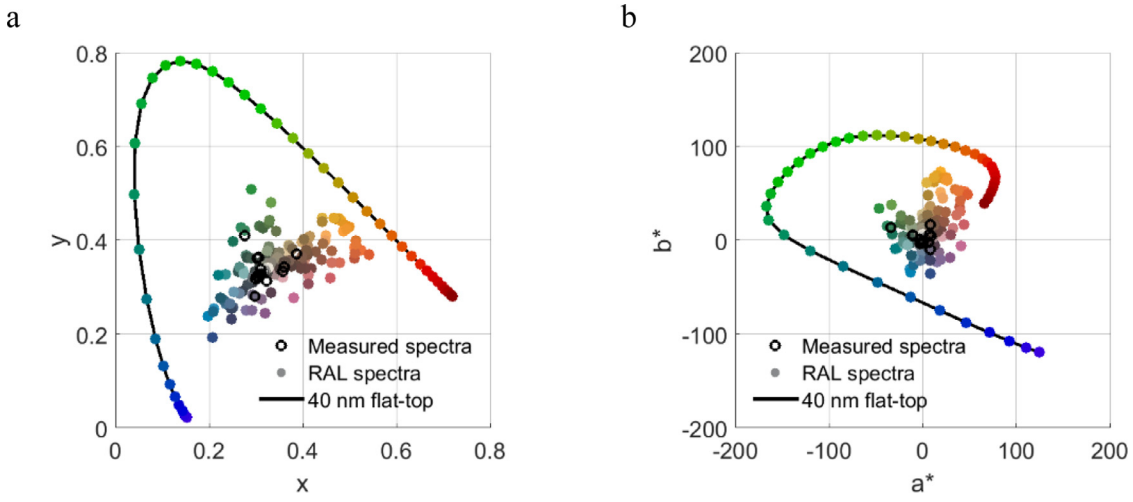

Fig. 16. Chromaticity diagram xy (a) and a*b* (b) showing the colour coordinates of measured spectra, RAL colours, and 40 nm flat-top band colours.

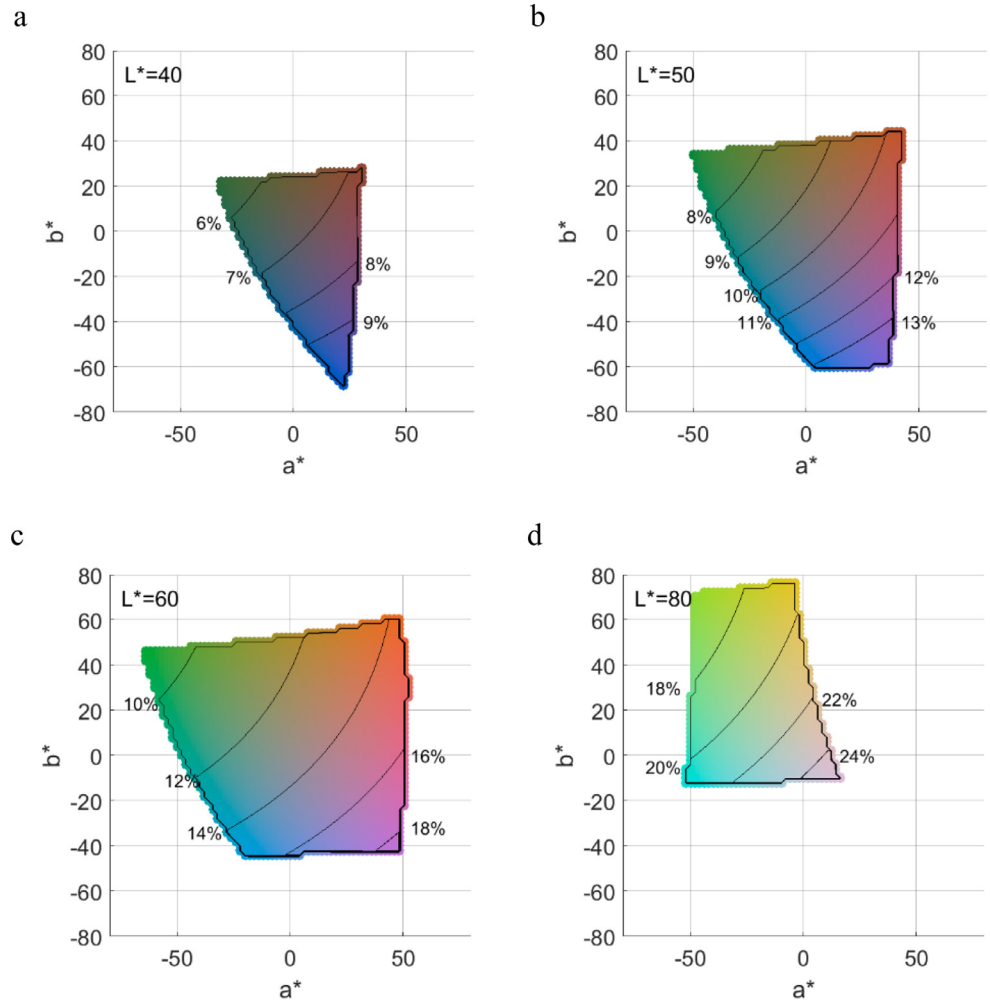

Fig. 17. Contour plot with lines of constant relative loss (P_{VIS}) for $L^* = 40$, 50, 60 and 80 corresponding to $Y = 0.11$, 0.18, 0.28 and 0.57, respectively.

To illustrate the range of colour coordinates that are represented in Fig. 15 the location in xy and a*b* chromaticity diagrams is displayed in Fig. 16. The colour coordinates (x,y and a*,b*) of the RAL spectra, measured spectra and 40 nm flat-top spectra are shown in Fig. 16.

A further illustration of importance of lightness L*, chroma (distance from $a^* = 0$, $b^* = 0$) and hue (angle in a*b* diagram) are given in Fig. 17. Here the same procedure has been applied to generate spectra as for the RAL colours. All colours that can be realized for each lightness ($L^* = 40$, 50, 60, 80) are shown in Fig. 17. A

contour map is overlaid on top to display the relative loss P_{VIS} for these colours.

The variation in P_{VIS} is smallest for the darkest colours. Fig. 17 also clearly illustrates the dependence on chroma and hue, and the fact that high chroma is only beneficial for a certain range of hues, in particular for green and yellow colours. For blue, pink and red colours, an increased chroma (and saturation) results in an increased loss.

It is of interest to predict the total relative loss P for a medium lightness $L = 50$. The relative loss in UV and NIR must then be added to P_{VIS} (Fig. 17). If we assume 4% baseline reflectance in UV and NIR, an additional 2% relative loss should be added, resulting in a total relative loss P ranging from 9 to 16% for $L^* = 50$. This loss is about 3 to 5 times higher than what can be achieved in the minimum loss case, 3.2%. (Fig. 8).

Our results for flat-top spectra are in good agreement with the results of Halme and Mäkinen [29], although they did not report their results in terms of a colour performance index. Their efficiency versus relative luminosity seems to correspond well with our results. They reported that for $Y < 0.25$ (corresponding to $L^* < 57$) the relative performance loss is less than 14% for almost the entire sRGB colour space. This is in close agreement with the result for flat-top 80 nm red and blue spectra as given in Fig. 11a.

Our results are more difficult to compare to the RAL results of Peharz and Ulm [30], since they have not analysed how the loss depend on lightness L^* or relative luminosity Y, but instead used a colour efficiency $C_{eff} = (X+Y+Z)(J_{sc}\text{-}J_{sc,ref})$. We do not see the purpose of using $X+Y+Z$ as a parameter in colour efficiency calculations. Instead, we have used Y for our calculation of colour performance index. The reason for this is that lightness L^* in the $L^*a^*b^*$ colour space is given by Y only (Eq. (8)). Instead of using $(J_{sc}\text{-}J_{sc,ref})$ for loss we have used the relative loss P in order to obtain a dimensionless CPI.

Peharz and Ulm [30] as well as Halme and Mäkinen [29] report results regarding the relative efficiency of white colours. Both use spectra composed of two flat-top spectra (pillbox spectra). This means that the white spectra are composed of a blue band and a green-yellow-red band. Peharz and Ulm [30] report relative losses of less than 20% for all RAL colours, including a white colour with $L^* = 95.3$ ($Y = 0.88$). Halme and Mäkinen [29] report results corresponding to a relative efficiency loss close to 28% for a white colour with $L^* = 96.4$ ($Y = 0.91$).

We found relative losses P_{VIS} of 42.5% for our grey in VIS model spectrum with L-value of 96 ($Y = 0.90$). This spectrum is less efficient than the spectra used by Peharz and Ulm [30] and Halme and Mäkinen [29], in that it reflects equally over the whole visible region (300–700 nm). The results for a white RAL colour (RAL 9016 Traffic White) with L^*-value of 95.3 ($Y = 0.88$) show a relative loss of 34.1%. The RAL model spectrum is more efficient than the grey in VIS model spectrum due to less reflectance near 300 and 700 nm. In our case of minimum loss with a single flat-top spectrum, an L^*-value of 96 results in a relative loss of 23.7%. However, this is not a white but rather a high chroma green colour. Our results based on the measured spectrum of the sample Vivid White (9) with L^*-value of 85.5 ($Y = 0.67$) show a relative loss P_{VIS} of 31.1% when losses in UV and NIR are excluded.

Since all three of our white spectra are more "realistic" than the white spectra used by Peharz and Ulm [30] and Halme and Mäkinen [29], we should expect slightly higher losses from our calculations. Our minimum loss case (high chroma green) should give relative loss values that are slightly better than the white spectra used by Peharz and Ulm [30] and Halme and Mäkinen [29]. Concluding from this, it seems that our findings are in good agreement with the results from Halme and Mäkinen [29] which report a relative efficiency loss close to 28%. On the contrary, our findings are not in agreement with the results from Peharz and Ulm [30]. Our calculated minimum loss result of 23.7% for a sample with $L^* = 96$ is higher than the losses reported by Peharz and Ulm [30]. The relative loss of only 20% for a white colour reported by Peharz and Ulm [30] should therefore not be possible according to our results.

The above results can be summarized and compared by the use of our colour performance index (CPI_{VIS}) which for these examples are the following: 4.40 (Peharz and Ulm [30]), 3.25 (Halme and Mäkinen [29],), 2.12 (Grey in VIS), 2.59 (RAL 9016 Traffic White), 2.16 (Vivid White) and 3.80 (minimum loss).

It is also worth noting the principle of metamerism, that many different spectra can produce the same colour coordinates. In our approach with three reflectance parameters to create the RAL spectra, the number of parameters is equal to the number of colour coordinates, and only one spectral solution exists for each colour. In the case of two flat-top spectral bands the number of parameters is 4, and care must be taken to ensure that the most energy efficient spectrum is selected. The relative loss for colours with identical colour coordinates but with different spectra may vary by more than a factor 3. The RAL colour Traffic Green, as an example, can be created with two narrow spectral bands centered at 435 and 550 nm or two broad spectral bands centered at 500 and 660 nm, resulting in relative loss of approximate 5 and 17%. The algorithm of Halme and Mäkinen [29] which is designed to minimize the total width of two spectral bands for a given colour will produce results close to the lowest relative loss.

There are several assumptions in the present model that needs to be pointed out. Firstly, it is assumed that there are no parasitic losses in the cover glass, encapsulation or in the reflecting elements that are responsible for creation of colour. Near lossless reflectance can be achieved by thin film interference from films of dielectric materials such as Si_3N_4, Al_2O_3 and TiO_2 [35]. If the colour is created by colour pigments that partly backscatter and partly absorb the incident radiation, the power loss will be greater than predicted by our model. A simplified model can be achieved by replacing the term $R(\lambda)$ in Eq. (17) with $R(\lambda)+A(\lambda)$. As an example, if the spectral absorbance equals the spectral reflectance, the relative efficiency loss will be twice as high. The challenge here is to either carry out measurements that determine the absorbance, or to have a good model that relates reflectance and absorbance. Due to our assumption of no absorbance, our results represent a lower limit of efficiency loss for a given reflectance.

An estimate of the influence of absorbance in the colouring layer can be given for the case of grey in UV–VIS-NIR case. A grey absorbance A in addition to the grey reflectance R will change the CPI from 1 to $R/(R+A)$, and the relative efficiency E from 1-R to 1-R-A. Another case that may be relevant is when the absorbance is not related to the colour generation. Then the loss should be included in the calculation of $J_{sc,ref}$ and separated from the absorbance caused by colour generation.

It is further assumed that colouring is not based on luminescent upshifting or downshifting [36]. Neither is the model valid for semi-transparent solar cell modules [37].

We have used a model and bandgap that is relevant for opaque crystalline silicon. Other PV technologies such as GaAs with a higher bandgap would give different results. The main difference is that the VIS part of the spectrum would represent a larger fraction of the energy generation, and hence reflection losses in VIS will then cause a larger relative efficiency loss. However, the concept of the proposed colour performance index is generic and can be applied to all opaque cell technologies. The CPI can thus be a useful figure of merit not only for comparison of different colours, but also for comparison of different colouring materials and technologies.

A similar analysis of different colours can also be carried out for thermal solar collectors [38]. The main difference to the CPI of Fig. 10 will be that the maximum CPI will be slightly higher, above

6, resulting from a smaller fraction of the usable energy within the visible. Furthermore, the CPI curve will be slightly redshifted due to the absence of $1/\lambda$ factor in the spectral response. The conclusion that green colours are more energy efficient than red and blue colours is therefore valid also for thermal solar collectors.

The present model and analysis can be useful in identifying important differences between the measured reflectance spectra, and how they translate into a high or low CPI. From Table 2 we see that sample 3, 7, 9, and 11 are the four samples with highest CPI. The main reason why sample 9 (Vivid White) has a high CPI is due to a NIR reflectance that is much lower than the VIS reflectance. The ratio between VIS and NIR reflectance is much higher for this sample all the other samples, as can be seen from Fig. 6. Sample 3, 7 and 11 also have better than average suppression of NIR reflectance but have in addition the benefit of being a green colour. These three samples have the best CPI_{VIS} values.

4. Conclusions

Commercially available coloured opaque solar cell modules have been analysed by measuring their reflectance properties and calculating their lightness and theoretical efficiency loss. Model spectra designed to create a larger variation in colour coordinates have also been analysed.

For opaque solar cell modules based on crystalline silicon cells, the lightness of the colour is the most important parameter affecting the loss. When comparing colours with the same lightness, hue is the most important parameter. Green colours are more energy efficient than grey, while blue and red colours are less energy efficient. The efficiency loss estimated from the measured reflectance spectra is typically three times higher than a minimum loss green module with optimum reflectance spectrum and the same lightness. We have established a colour performance index (CPI) that is the fraction between luminous reflectance Y and relative loss P as a figure of merit for comparison of different colours. This CPI is as high as 5.75 for a minimum loss green module, while the measured modules range from 0.9 up to 1.6. For a medium lightness $L^* = 50$ ($Y = 0.18$), we find that a minimum loss green colour can have a loss as low as 3.2% while more realistic spectra of a range of colours predict a relative loss varying from 9 to 16%.

We have also highlighted the importance of keeping the near infrared (NIR) reflectance low. In solar cell modules based on crystalline silicon, about half of the energy is generated from the NIR radiation. Our results also show that the characterized modules introduce undesired reflections in the NIR region that may contribute more to the efficiency loss than the visible reflectance. Development of low-cost and low-loss colouring techniques that can create solar cell modules with specific colours with minimized NIR reflectance is therefore of high importance.

We believe that the losses introduced by adding lightness and colour to the modules will be considered acceptable for many building applications, as long as care is taken by the module manufacturers to minimize this loss. For most buildings black surfaces are not desired, and only lighter and coloured solar modules will be considered. Efficient and aesthetically pleasing coloured solar cell modules therefore represent an important contribution towards more widespread use of BIPV in buildings.

Acknowledgements

The authors gratefully acknowledge the support from the Research Council of Norway through the project Building Integrated Photovoltaics for Norway (RCN project number 244031) and The Research centre for Sustainable Solar Cell Technology (RCN project number 257639).

Supplementary materials

Supplementary material associated with this article can be found, in the online version, at doi:10.1016/j.enbuild.2019.109623.

References

[1] A.G. Hestnes, Building integration of solar energy systems, Solar Energy 67 (1999) 181–187.
[2] B.P. Jelle, C. Breivik, H.D. Røkenes, Building integrated photovoltaic products: a state-of-the-art review and future research opportunities, Solar Energy Mater. Solar Cells 100 (2012) 69–96.
[3] P. Heinstein, C. Ballif, L.E. Perret-Aebi, Building integrated photovoltaics (BIPV): review, potentials, barriers and myths, Green 3 (2) (2013) 125–156.
[4] A.K. Shukla, K. Sudhakar, P. Baredar, A comprehensive review on design of building integrated photovoltaic system, Energy Build. 128 (2016) 99–110.
[5] M. Tripathy, P.K. Sadhu, S.K. Panda, A critical review on building integrated photovoltaic products and their applications, Renew. Sustain. Energy Rev. 61 (2016) 451–465.
[6] B.P. Jelle, Building integrated photovoltaics: a concise description of the current state of the art and possible research pathways, Energies 9 (2016) 1–30 Article no. 21.
[7] C. Ballif, L.E. Perret-Aebi, S. Lufkin, E. Rey, Integrated thinking for photovoltaics in buildings, Nat. Energy 3 (2018) 438–442.
[8] J. Palm, L. Tautenhahn, J. Weick, R. Kalio, J. Kullmann, A. Heiland, S. Grünsteidl, N. Schmidt, P. Borowski, F. Karg, BIPV modules: critical requirements and customization in manufacturing, IEEE 7th World Conference on Photovoltaic Energy Conversion (WCPEC), 2018.
[9] K. Farkas, in: Architectural Integration of Photovoltaics, 2013, NTNU, Trondheim, 2013, p. 78. PhD thesis.
[10] J. Shih, S.-.L. Lai, H.-.T. Cheng, The principle and applications of colored solar cells, Adv. Mat. Res. (2013) 420–425.
[11] K. Ding, X. Zhang, L. Ning, Z. Shao, P. Xiao, A. Ho-Baillie, X. Zhang, J. Jie, Hue tunable, high color saturation and high-efficiency graphene/silicon heterojunction solar cells with MgF_2/ZnS double anti-reflection layer, Nano Energy, 46 (2018) 257–265.
[12] J.H. Selj, T.T. Mongstad, R. Søndenå, E.S. Marstein, Reduction of losses in colored solar cells with multilayer antireflection coating, Solar Energy Mater. Solar Cells 95 (2011) 2576–2582.
[13] M. Amara, F. Mandorlo, R. Couderc, F. Gerenton, M. Lemiti, Temperature and color management of silicon solar cells for building integrated photovoltaic, EPJ Photovoltaics 9 (2018) 1.
[14] N. Jolissaint, R. Hanbali, J.-.C. Hadorn, A. Schüler, Colored solar facades for buildings, Energy Procedia 122 (2017) 175–180.
[15] M. Li, Zeng L, Y. Chen, L. Zhuang, X. Wang, H. Shen, Realization of colored multicrystalline cells with sio2/sinx:H double layer antireflection coatings, Int. J. Photoenergy (2013) 352473.
[16] L. Zeng, M. Li, Y. Chen, H. Shen, A simplified method to modulate colors on industrial multicrystalline silicon solar cells with reduced current losses, Solar Energy 103 (2014) 343–349.
[17] J. Escarre, H.Y. Li, L. Sansonnens, F. Galliano, G. Cattaneo, P. Heinstein, S. Nicolay, J. Bailat, S. Eberhard, C. Ballif, L.E. Perret-Aebi, When pv modules are becoming real building elements: white solar module, a revolution for BIPV, IEEE 42nd Photovoltaic Specialists Conference (PVSC), 2015.
[18] S. Mertin, V. Hody-Le Caer, M. Joly, I. Mack, P. Oelhafen, J.L. Scartezzini, A. Schüler, Reactively sputtered coatings on architectural glazing for coloured active soalr thermal facades, Energy Build. (2014) 764–770.
[19] F. Frontini, P. Bonomo, E. Saretta, T. Weber, J. Berghold, Indoor and outdoor characterization of innovative colored bipv modules for façade application, 32nd European Photovoltaic Solar Energy Conference and Exhibition, 2016.
[20] M. Mittag, C. Kutter, M. Ebert, H.R. Wilson, U. Eitner, Power loss through decorative elements in the front glazing of BIPV modules, 33rd European PV Solar Energy Conference and Exhibition, 25-29 September, 2017.
[21] L.H. Slooff, J.A.M. van Roosmalen, L.A.G. Okel, T. de Vries, T. Minderhoud, G. Gijzen, T. Sepers, A. Versluis, F. Frumau, M. Rietbergen, L. Polinder, E.M.B. Heller, F. de Vries, An architectural approach for improving aesthetics of PV, (2017), 33rd European PV Solar Energy Conference and Exhibition, 25-29 September, 2017.
[22] K.T. Lee, J.Y. Lee, T. Xu, H.J. Park, L.J. Guo, Colored dual functional photovoltaic cells, J. Opt. 18 (2016) 064003.
[23] G. Peharz, K. Berger, B. Kubicek, M. Aichinger, M. Grobbauer, J. Gratzer, W. Nemitz, B. Grosschädl, C. Auer, C. Prielt, W. Waldhauser, G.C. Eder, Application of plasmonic coloring for making building integrated pv modules comprising of green solar cells, Renew. Energy 109 (2017) 542–550.
[24] E.S. Arinze, B. Qiu, N. Palmquist, Y. Cheng, Y. Lin, G. Nyirjesy, Gary Qian, S.M. Thon, Color-tuned and transparent colloidal quantum dot solar cells via optimized multilayer interference, Opt Express 25 (2017) 4.
[25] B. Bläsi, T. Kroyer, O. Höhn, M. Wiese, C. Ferrara, U. Eitner, T.E. Kuhn, Morpho butterfly inspired coloured BIPV modules, 33rd European PV Solar Energy Conference and Exhibition, 25–29 September, 2017.
[26] W. Zhang, M. Anya, G. Lozano, M.E. Calco, M.B. Johnston, H. Miguez, H.J. Snaith, Highly efficient Perovskite solar cells with tunable structural color, Nano Lett. 15 (2015) 1698–1702.

[27] A. Soman, A. Antony, Colored solar cells with spectrally selective photonic crystal reflectors for application in building integrated photovoltaics, Solar Energy 188 (2019) 1–8.
[28] V. Neder, S.L. Luxembourg, A. Polman, Efficient coored silicon modules using integrated resonant dielectric nanoscatterers, Appl. Phus. Lett. 111 (2017) 073902.
[29] J. Halme, P. Mäkinen, Theoretical efficiency limits of ideal coloured opaque photovoltaics, Energy Environ. Sci. (2019), doi:10.1039/C8EE03161D.
[30] P.G. Peharz, A. Ulm, Quantifying the influence of colors on the performance of c-Si photovoltaic devices, Renew. Energy 129 (2018) 299–308.
[31] Wyszecki Günter, W.S. Stiles, Color Science - Concepts and Methods, Quantitative Data and Formulae, 2nd ed, Wiley-Interscience, 2000.
[32] CIE, International commission on illumination, Colorimetry, 2004 Technical reportCIE15:2004.
[33] J. Nelson, The Physics of Solar Cells, Imperial College Press, 2003.
[34] https://en.wikipedia.org/wiki/List_of_RAL_colors.
[35] H.A. MacLeod, Thin Film Optical Filters, Taylor & Francis, BristolPhiladephia, 2001.
[36] X. Huang, S. Han, W. Huang, X. Liu, Enhancing solar cell efficiency: the search for luminescent materials as spectral converters, ChemSocRev 42 (2013) 173.
[37] D.H. Shin, S.-.H. Choi, Recent studies of semitransparent solar cells, Coatings 8 (2018) 329.
[38] A. Schüler, C. Roeckerr, J.-.L. Scartezzini, J. Boudalen, I.R. Videnovic, R.S.-C. Ho, P. Oelhafen, On the feasibility of colored glazed thermal collectors based on thin film interference filters, Solar Energy Mater. Solar Cells 84 (2004) 241–254.